SWI/SNF-Mediated Lineage Determination in Mesenchymal Stem Cells Confers Resistance to Osteoporosis

STEM CELLS®

TISSUE-SPECIFIC STEM CELLS

SWI/SNF-Mediated Lineage Determination in Mesenchymal Stem Cells Confers Resistance to Osteoporosis

KEVIN HONG NGUYEN, FUHUA XU, STEPHEN FLOWERS, EDEK A.J. WILLIAMS, J. CHRISTOPHER FRITTON, ELIZABETH MORAN

Key Words. SWI/SNF • mammalian brahma, BRM • Osteoblasts • Adipocytes • Mesenchymal stem cells • Osteoporosis

Department of Orthopaedics, New Jersey Medical School, Rutgers, The State University of New Jersey, Newark, New Jersey, USA

Correspondence: Elizabeth Moran, Ph.D., Department of Orthopaedics, New Jersey Medical School, Rutgers, The State University of New Jersey, 205 South Orange Avenue, Newark, New Jersey 07103, USA. Telephone: 973-972-5854; Fax: 973-972-1875; e-mail: moranel@njms.rutgers.edu

Received August 14, 2014; accepted for publication March 24, 2015; first published online in STEM CELLS *EXPRESS* June 8, 2015.

1066-5099/2015/$30.00/0

http://dx.doi.org/10.1002/stem.2064

ABSTRACT

Redirecting the adipogenic potential of bone marrow-derived mesenchymal stem cells to other lineages, particularly osteoblasts, is a key goal in regenerative medicine. Controlling lineage selection through chromatin remodeling complexes such as SWI/SNF, which act coordinately to establish new patterns of gene expression, would be a desirable intervention point, but the requirement for the complex in essentially every lineage pathway has generally precluded selectivity. However, a novel approach now appears possible by targeting the subset of SWI/SNF powered by the alternative ATPase, mammalian brahma (BRM). BRM is not required for development, which has hindered understanding of its contributions, but knockdown genetics here, designed to explore the hypothesis that BRM-SWI/SNF has different regulatory roles in different mesenchymal stem cell lineages, shows that depleting BRM from mesenchymal stem cells has a dramatic effect on the balance of lineage selection between osteoblasts and adipocytes. BRM depletion enhances the proportion of cells expressing markers of osteoblast precursors at the expense of cells able to differentiate along the adipocyte lineage. This effect is evident in primary bone marrow stromal cells as well as in established cell culture models. The altered precursor balance has major physiological significance, which becomes apparent as protection against age-related osteoporosis and as reduced bone marrow adiposity in adult BRM-null mice.
STEM CELLS *2015;33:3028–3038*

INTRODUCTION

Osteoblasts and adipocytes are among the lineages that arise from multipotent mesenchymal stem cells in the bone marrow stroma. Commitment to one or the other has particular significance in skeletal diseases such as osteoporosis, which increases with age partly due to an increasing tendency of bone marrow stromal cells (BMSCs) to differentiate into adipocytes at the expense of osteoblasts, and is correspondingly characterized by accumulation of fat in the bone marrow compartment. Increased marrow adiposity generally accompanies physiological conditions leading to bone loss [1, 2], and redirecting the adipogenic potential of BMSC to osteoblasts is a key goal in regenerative medicine.

Regulation of gene expression patterns during differentiation of any cell lineage requires cooperation with the SWI/SNF chromatin-remodeling complex [3]. SWI/SNF is a complex of approximately 10 proteins, discovered and named in yeast, where mutants fail to undergo the mating type Switch and become Sucrose NonFermenters. The SWI/SNF complex is conserved in evolution through higher eukaryotes, and the basis of its action in gene expression is an ATPase-powered ability to alter nucleosome positioning to provide promoter access for activation or repression factors near transcriptional start sites. Because this activity is fundamental to development, the complex is potentially a major target for control of tissue regeneration. The complex is ubiquitous and can support either activation or repression functions, in part because it exists in most mammalian cells in different configurations with respect to alternative subunits [3–5]. Very little is known about the role of alternative SWI/SNF configurations in control of lineage selection, especially in mesenchymal stem cells (MSC). Mammalian SWI/SNF is powered by either of two independent ATPases, BRM or BRG1. The importance of the alternative ATPases to mammalian development is vastly different; BRG1-null mice die early in embryogenesis, while BRM-null mice grow to healthy adulthood [6, 7]. BRG1 is required for tissue-specific gene expression in

every model system tested [3, 8–12], but the role of BRM is more nuanced, presumably offering a fine-tuning function. Direct comparison of the roles of BRG1 and BRM by individual shRNA targeting in a preosteoblast model revealed that BRM-SWI/SNF exerts a counteracting function to the required role of BRG1 in osteoblast differentiation. BRM-SWI/SNF directly occupies osteogenic promoters before induction, and is required to maintain effective co-occupation by repressor factors that include histone-modifying enzymes, as well as repressor members of the E2F transcription factor family and their binding partner p130 [13–16]. BRM-deficient preosteoblasts thus show premature expression of osteoblast differentiation markers [13]. The role of BRM-containing SWI/SNF as a counterforce to differentiation was unexpected, and raises the question of how BRM-SWI/SNF affects multipotent cells before osteoblast commitment. Our aim here is to understand the biological effect of BRM-SWI/SNF at an earlier level of commitment, when the decision is made between the osteoblast and adipocyte lineages.

The few reports that have considered the role of SWI/SNF in adipogenesis established a required role for the complex [17–19]. Interestingly though, BRM appears to play a positive role in adipogenesis similar to BRG1 [18]. The authors noted that the dominant-negative approach used to inhibit BRM versus BRG1 might be complicated by cross-competition, but an alternative approach here using shRNA-targeting supports the positive role of BRM-SWI/SNF in pre-adipocyte differentiation. These contrasting effects in committed progenitors do not mean that BRM-SWI/SNF plays a lineage-determinant role in stem cells, but this important possibility has not been addressed, and a positive finding could have major implications for disorders of bone formation. Examining this hypothesis in the C3H10T1/2 cell model of mesenchymal stem cells reveals a potent effect of BRM deficiency on lineage selection. BRM-depleted C3H10T1/2 cells show enhanced expression of osteogenic markers and impaired differentiation along the adipocyte pathway. Primary BMSCs harvested from BRM-null mice are similarly enriched for cells expressing markers of osteoblast precursors and simultaneously impoverished for adipogenic potential. Moreover, the altered precursor balance has major physiological effects in the whole animal. BRM-null mice show reduced bone marrow adiposity and are strikingly resistant to age-related osteoporosis.

Materials and Methods

Materials

Puromycin, oil red O, and insulin were obtained from Sigma Chemical Co. (St. Louis, MO, https://www.sigmaaldrich.com); dexamethasone and 3-isobutyl-1-methylxanthine (IBMX) from Acros Organics (Fair Lawn, NJ, www.acros.com/); fetal bovine serum (FBS) from Atlanta Biologicals (Norcross, GA, https://www.atlantabio.com/); and buffered Z-fix formalin from Thermo-Fisher (Waltham, MA, www.thermofisher.com/).

Cell Lines

Low passage 3T3-L1 and C3H10T1/2 cells (clone 8) were obtained from the ATCC and cultured, respectively, in Dulbecco's modified Eagle's medium (DMEM) or Eagle's basal medium, plus 10% FBS and 1% penicillin/streptomycin. For adipocyte differentiation, 2 days post-confluent 3T3-L1 cells were supplemented with 1 μM dexamethasone, 0.5 mM IBMX, and 1 μg/ml insulin for 2 days, then with 1 μg/ml insulin alone for 2 days, then maintained in DMEM plus 10% FBS. C3H10T1/2 cells were induced similarly, but with 5 μg/ml insulin. Lipid storage was visualized by oil red O staining of formalin-fixed cells. Stable BRM and BRG1 knockdown lines were selected in puromycin (3 μg/ml) after cotransfection with pSUPER vectors encoding BRM or BRG1 specific shRNA sequences described previously [13, 15]. Culture of MC3T3-E1 cells and induction of their differentiation in the presence of ascorbic acid and β-glycerol phosphate were performed as described [13, 15].

RNA and Protein Expression

Protein immunoblotting methods were described previously [11]; antibodies specific for RUNX2 (S-19, sc-12488) and HSC70 (B-6, sc-7298) were obtained from Santa Cruz Biotechnology (Santa Cruz, CA, www.scbt.com/). RNA expression was evaluated by quantitative reverse transcription polymerase chain reaction (qRT-PCR). The qRT-PCR methodology and the primers for *Smarca4* (BRG1), *Alpl*, *Fgfr2*, and *Gapdh* have been described previously [14, 15]. Other primers used are: BRM (*Smarca2*): forward: 5′-GTCCAGTAGGCAGGAAACCGA-3′, reverse: 5′-ACTGAGAGCCTCTGGCACTGTA-3′; *Pparg2:* forward: 5′-GGGGTGATGTGTTTGAACTTG-3′, reverse: 5′-CAGGAAAGACAACAGACAAAT-3′; *Cebpa:* forward: 5′-GTGCTGGAGTTGACCAGTGA-3′, reverse: 5′-AAACCATCCTCTGGGTCTCC-3′; *Cebpb*; forward: 5′-CAAGCTGAGCGACGAGTACA-3′, reverse: 5′-CAGCTGCTCCACCTTCTTCT-3′; *Fabp4:* forward: 5′-GACAGCTCCTCCTCGAAGGTT-3′, reverse: 5′-GGTTCCCACAAAGGGATCAC-3′; *Runx2:* forward: 5′-GCCGGGAATGATGAGAACTA-3′, reverse: 5′-GGACCGTCCACTGTCACTTT-3′; Osterix (*Sp7*): forward 5′-ATGGCGTCCTCTCTGCTTG-3′, reverse 5′-TGAAAGGTCAGCGTATGGCTT-3′.

All qRT-PCR assays from established cell lines are shown as the mean of triplicates $\pm$ SEM. Each assay shown is representative of three or more independent trials. As further controls, assays were performed in at least two independently derived BRM-depleted lines, which are reported separately. Key findings were confirmed in primary cells from the mouse model.

BRM-Null Mice and Primary BMSCs

Brm$^{-/-}$ mice have been described [3] and were maintained at NJMS in an AAALAC-accredited facility according to IACUC-approved protocols. Primary BMSCs were obtained by flushing femurs of 21–35 day old mice with 5 ml of DMEM containing 15% FBS. Typically, material from four femurs was combined in one 60-mm culture dish and left to attach for 72 hours. Nonadherent cells were removed, and culture medium was replenished every 2–3 days. At day 7, the cells were trypsinized and divided 1:2. Eight days later, when still subconfluent, one plate was assayed by in situ staining for alkaline phosphatase activity as described previously [13], and the other was induced for adipocyte differentiation by treatment with 1 μM dexamethasone, 0.5 mM IBMX, and 5 μg/ml insulin for 2 days, followed by maintenance in culture medium supplemented with 1 μM dexamethasone and 5 μg/ml insulin, replenished every 2–3 days. At day 12 postinduction adipocyte formation was probed by oil red O staining. RNA was isolated from BMSC taken from mice ranging from 1 to 4 months in age, plated as above and harvested from nonconfluent cultures at day 7 post-plating.

Histology

Tibias from 12 wild type and 12 BRM-null adult mice, (equal numbers of each sex in each genotype), all approximately 4 months old (range: 106–143 days) were formalin fixed (>24 hours), formic acid decalcified (>24 hours), paraffin embedded, sectioned (5 μm thickness in frontal plane) and stained by hematoxylin and eosin (H&E) using standard protocols. Sections (1–3 per tibia) were bright-field imaged (Eclipse 50i and Microphot-FXA, Nikon) and stitched together (Adobe Photoshop CS5). Marrow area was traced and adipocytes counted with a pen/tablet workstation (Wacom Cintiq 21UX). Sections were analyzed for number of adipocytes per unit marrow area (NIH ImageJ) by observers blinded to the genotype of the samples.

Microcomputed Tomography

Microcomputed tomography (Bruker SkyScan 1172 μCT; 80 kV, 120 μA) of right femurs was carried out at an isotropic voxel resolution of 8 μm. Density calibration phantoms (0.25 and 0.75 g/cm^3) were also scanned to enable tissue mineral density (TMD) calculations. Femoral cortical bone properties, measured at the mid-diaphysis by averaging 10 slices, were analyzed in CTAn software (Bruker) by observers blinded to the genotype of the samples. The average age of the 6-month-old set ($n = 4$ animals of each genotype) was 185.5 days for wild type and 199.8 days for BRM-null. The average age of the 18-month-old set ($n = 5$ animals of each genotype) was 558.9 days for wild type and 559.5 days for BRM-null.

Results

Adipocyte Differentiation Is Impaired Early in Induction in BRM-Depleted 3T3-L1 Cells

Dominant-negative inhibition of either BRM or BRG1 blocks the ability of the transcription factor C/EBPα to induce adipogenesis in mouse NIH3T3 fibroblasts [18]. The positive role of BRM in adipocyte differentiation was examined further here in the 3T3-L1 committed pre-adipocyte cell line. A selective shRNA approach was used to derive individual lines stably depleted of BRM or BRG1. Two lines targeting each ATPase were isolated independently (BRM.KD.C182 and BRM.KD.C119 as well as BRG1.KD.C112 and BRG1.KD.C111). Each line shows substantially reduced expression of the intended target, with the alternative ATPase relatively unaffected (Fig. 1A). To monitor adipogenic potential, cells were induced for 10 days, and mature adipocytes were identified as spherical cells filled with lipid droplets that stain with oil red O. Typical results are

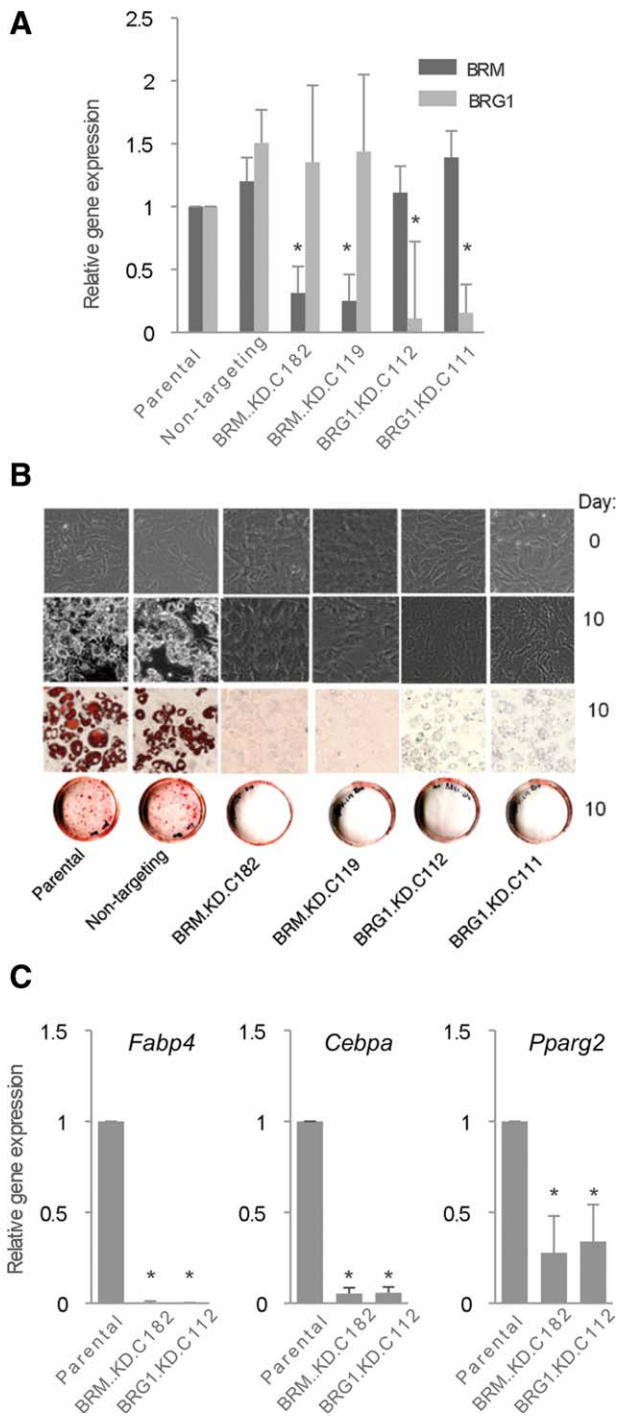

Figure 1. Impaired adipocyte differentiation in BRM depleted 3T3-L1 cells. BRM depletion does not affect BRG1 expression, but impairs adipogenesis and the induction of adipogenic genes in 3T3-L1 pre-adipocytes. **(A):** Expression of the genes encoding BRM and BRG1 in the respective shRNA-targeted lines was determined by quantitative reverse transcription polymerase chain reaction (qRT-PCR) normalized to *Gapdh* expression. Shown are mean ± SEM. Asterisks signify a significant change relative to the parental value ($p \leq 0.05$ for three or more independent assays), BRM expression is significantly reduced in both BRM-targeted lines while BRG1 expression is not significantly changed. Conversely, BRG1 expression is significantly reduced in both BRG1-targeted lines, while BRM expression is not significantly changed. **(B):** Oil red O staining was used to assess adipogenesis at 0 and 10 days post-induction. Two independent BRM-depleted lines and two independent BRG1-depleted lines were compared with parental 3T3-L1 cells and a control line isolated after transfection with a nontargeting shRNA sequence. The depleted lines do not show a lipid-storing morphology under phase microscopy (digital image captured with a 20× objective on an EVOS XL system), or without magnification on the 6-cm monolayers. **(C):** Expression of adipogenic markers after 8 days of induction was compared in parental, BRM-depleted, and BRG1-depleted 3T3-L1 cells. Expression was determined by qRT-PCR, normalized to *Gapdh* expression. Shown are mean ± SEM. Asterisks indicate a significant difference relative to the parental value ($p \leq 0.05$ for three or more independent assays).

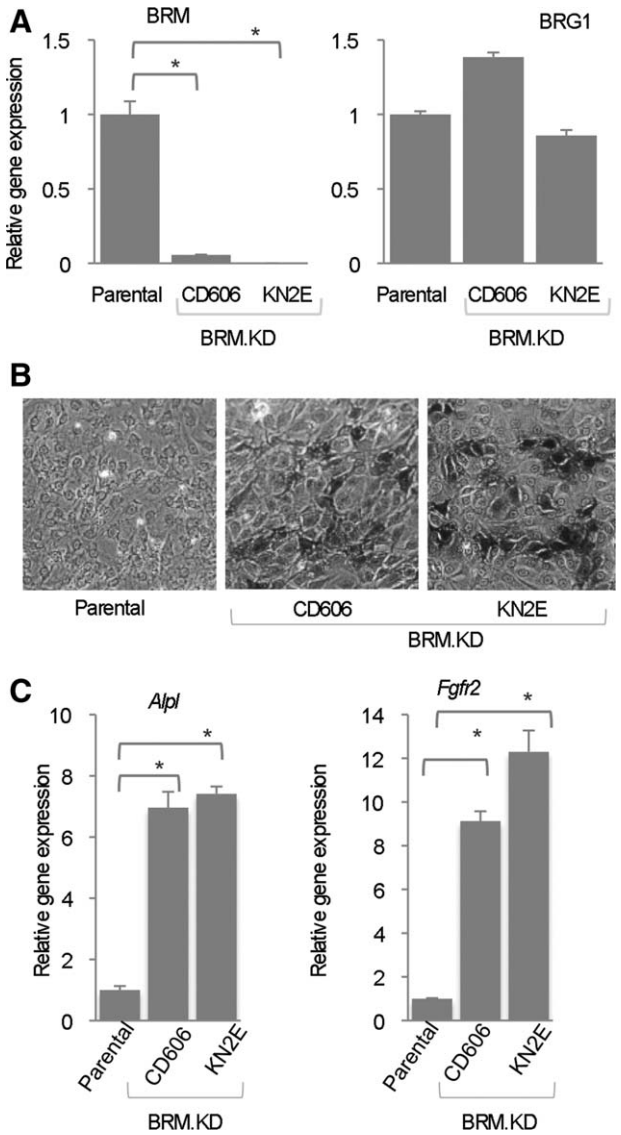

Figure 2. BRM depletion enhances expression of osteoblast markers in the C3H10T1/2 mesenchymal stem cell model. **(A):** Expression of the genes encoding BRM and BRG1 was determined by quantitative reverse transcription polymerase chain reaction (qRT-PCR) in two independently isolated BRM-depleted lines (BRM.KD CD606 and KNE2). Shown are mean values normalized to *Gapdh* expression relative to parental C3H10T1/2 cells; the error bars represent the SEM ($n = 3$). Asterisks indicate a significant difference compared with the parental value as described in Figure 1. BRM expression in the BRM-targeted lines is sharply reduced, with no significant change in BRG1 expression. **(B):** Staining to reveal alkaline phosphatase activity, a marker of the osteoblast progenitor phenotype, shows a markedly increased number of positive cells in the BRM-depleted lines compared with parental C3H10T1/2 cells plated in parallel. Images were captured on an EVOS XL system with a 4× objective. **(C):** Expression of *Alpl* (encoding alkaline phosphatase) and *Fgfr2* (encoding the type 2 FGF receptor) is elevated in BRM-depleted cells relative to parental C3H10T1/2 cells. Expression was determined by qRT-PCR, as described in panel **(A)**. Asterisks indicate a significant difference compared with the parental value as described in Figure 1.

shown for each line compared with parental cells, or to cells transfected with a nontargeting control shRNA sequence (Fig. 1B). Lipid accumulation fails to occur detectably when either BRM or BRG1 is depleted, affirming that each subset of SWI/SNF contributes positively to adipocyte differentiation.

The respective contribution of the alternative ATPases to expression of individual adipogenic genes has not been examined previously. Adipogenesis is a well-characterized differentiation program in which key transcriptional regulators such as C/EBPα and PPARγ2 are induced early, and act directly to induce many adipocyte-specific genes such as *Fabp4*, which encodes the lipid transporter aP2, a highly expressed late stage adipocyte marker [20, 21]. Consistent with the lack of lipid accumulation, induction of *Fabp4* is severely impaired in both BRM and BRG1 depleted cells (Fig. 1C). Notably, *Cebpa* and *Pparg*, which encode the critical early transcription factors C/EBPα and PPARγ2, both fail to induce normally in cells depleted of either ATPase, indicating that both ATPases contribute significantly to activation of the initial transcription factor cascade. C/EBPα induction is among the earliest events at the onset of adipocyte differentiation [20, 21], and its mutual dependence on both ATPases indicates that both play required roles very early in the adipogenic program. This places the effect of BRM upstream of PPARγ2 as well; this nuclear hormone receptor is considered to play a key role in the reciprocal regulation of osteoblasts and adipocytes [22–24].

BRM Is a Determinant of Lineage Selection in a Multipotent Mesenchymal Stem Cell Model

The key question of whether targeting BRM can alter the balance of lineage selection in stem cells before commitment was addressed by deriving BRM-depleted lines from C3H10T1/2 cells, an established model of multipotent mesenchymal stem cells. Two BRM-depleted lines (CD606 and KN2E) were isolated independently and amplified for study. Each shows substantially reduced expression of BRM with relatively little effect on BRG1 (Fig. 2A).

A major early marker of the osteoblast progenitor phenotype is increased alkaline phosphatase activity. This enzyme is required for extracellular mineralization, and localizes to the outer cell membrane where its activity can be detected in a colorimetric assay forming a dark precipitate. C3H10T1/2 cells typically do not evince an osteoblast phenotype unless cells are grown to confluency and exposed to osteogenic induction factors such as bone morphogenic proteins [25]. However, assessment of BRM-depleted C3H10T1/2 cells permitted to reach confluency in the absence of induction by exogenous factors shows numerous cells that display heightened alkaline phosphatase activity indicative of enhanced osteogenic potential (Fig. 2B).

A qRT-PCR probe confirms constitutively elevated expression of the alkaline phosphatase-encoding gene, *Alpl,* even in subconfluent BRM-depleted C3H10T1/2 cells (Fig. 2C). Another gene of interest is *Fgfr2,* encoding fibroblast growth factor receptor type 2 [13, 15]. FGFR2 came to the attention of bone biologists because human germ-line mutations that activate the tyrosine kinase activity of the receptor cause premature differentiation of pre-osteoblasts, manifesting as craniosynostosis syndromes [26, 27]. Overexpression of *Fgfr2* may influence lineage choice towards osteoblastogenesis over adipogenesis [28], and a focused gene array analysis identified *Fgfr2* as a direct target of SWI/SNF in pre-osteoblasts [13, 15]. Analysis here by qRT-PCR shows *Fgfr2* is not highly expressed

in C3H10T1/2 cells, but undergoes about 10-fold induction following BRM depletion (Fig. 2C).

The same BRM-depleted C3H10T1/2 cell populations that showed enhanced expression of osteogenic markers were assessed for adipogenic potential (Fig. 3A). Virtually no lipid containing cells were detectable by light microscopy at 8 days post-induction when the parental line already shows abundant lipid accumulation. Very little oil red O staining is apparent in the monolayers even when induction is extended to day 12. Expression of adipogenic markers assayed at post-induction day 2 (for early markers) or day 8 (for the late-stage marker aP2/*Fabp4*) similarly shows markedly impaired induction in the BRM-depleted lines (Fig. 3B). Notably, even constitutive (day 0) expression of the early adipogenic transcription factors encoded by *Cebpa* and *Cebpb* is substantially reduced with BRM deficiency; this is seen in the same RNA preparations showing increased osteogenic gene expression in Figure 2. Thus, a reduction in BRM levels in the mesenchymal stem cell precursor model strongly impedes differentiation along the adipocyte lineage at a very early stage, and favors differentiation along the osteoblast lineage.

BRM-Depleted Cells Establish Commitment to the Osteoblast Lineage Without Undergoing Further Differentiation

The osteogenic markers upregulated in the BRM-depleted cells are associated with osteoblast commitment, but commitment does not constitute differentiation to the mature osteoblast phenotype. The transition from a committed osteoblast progenitor to a defined pre-osteoblast is marked by increased expression of the transcription factors RUNX2 and osterix (encoded by the *Sp7 gene*) [29]. We reported previously that *Runx2* expression is not dependent on SWI/SNF in the pre-osteoblast cell model, MC3T3-E1 cells, where expression is already active [13]. The question remains whether BRM depletion in the stem cells results in induction of either factor. Expression was examined by qRT-PCR in the BRM-depleted lines, and compared with levels in the MC3T3-E1 cells (Fig. 4A). Osterix is well expressed in MC3T3-E1 cells, but expression is much lower in the C3H10T1/2 cells, and is not appreciably increased by depletion of BRM. *Runx2* expression in C3H10T1/2 cells is also not increased by BRM depletion. This is consistent with models in which osterix expression is activated by RUNX2, and in which RUNX2 is not highly active in C3H10T1/2 cells [29]. Differential expression of *Runx2* between the stem cell model and the pre-osteoblast model is little more than twofold, but RUNX2 is also regulated at the protein level [29]. Western blotting (Fig. 4B) shows the difference in RUNX2 levels between C3H10T1/2 and MC3T3-E1 cells, and confirms that RUNX2 is not appreciably increased by BRM depletion. These gene expression patterns indicate that BRM depletion increases the commitment of the stem cell pool to the osteoblast lineage, but does not actually cause the cells to differentiate even as far as the pre-osteoblast stage defined by RUNX2-dependent upregulation of osterix expression.

Given that engineering of BRM deficiency favors differentiation along the osteoblast lineage, we considered whether BRM itself is downregulated during osteoblast differentiation. BRM expression was assessed in MC3T3-E1 cells at time points representative of the pre-osteoblast stage (day 0 of induction), the matrix-forming stage (day 7), and late-stage differentiation when mineralization occurs (day 14). Analysis by qRT-PCR indicates that BRM expression, like BRG1 expression, stays relatively constant throughout differentiation (Fig. 4C). This is not necessarily unexpected. Relief of BRM-mediated repression occurs by sequential dissociation of BRM-SWI/SNF from the promoters of osteogenic genes like alkaline phosphatase [13–16], a process that does not in itself require downregulation of BRM. BRM and BRG1 levels vary moderately at some developmental stages, but both have broad roles in SWI/SNF-mediated gene regulation not limited to tissue-specific genes [3, 30, 31], so there is no a priori reason that BRM expression would be down regulated at this point.

Altered Osteoblast Versus Adipogenic Potential in Primary BRM-Deficient BMSC

The physiological significance of targeting BRM was examined in a whole animal model. BRM-null mice were developed years ago and are notable for showing little overt phenotype in comparison with BRG1-null mice, which die early in embryogenesis [6, 7]. BRM-null mice attain normal weight and show no evidence of skeletal abnormalities [6]. Yet the cell culture findings imply the balance of osteoblast versus adipocyte determination would be altered in the BRM-null bone marrow stem cell pool. To address this question, BMSC were harvested from the femurs of BRM-null mice and their wild type counterparts, and plated at low density. Parallel monolayers were assayed for alkaline phosphatase activity without induction, or were induced for 12 days with adipocyte induction medium. Micrographs comparing the osteoblast and adipocyte forming potential are shown in Figure 5A. The results echo the findings in the C3H10T1/2 cell model. Primary BMSC from BRM-null mice, without induction, contain a markedly greater number of more-intensely staining alkaline phosphatase-positive cells than BMSC from their wild type counterparts (upper panels). Cell counts from four independent experiments are summarized in the graph below; BMSC from BRM-null mice show 16.8-fold more alkaline phosphatase positive cells than BMSC from wild type mice. When aliquots of the same cells were treated with adipocyte induction medium, an oil red O positive signal developed in cells from wild type mice but not in cells derived from BRM-null mice. The positive cells occur in small clusters, reflective of the short proliferative phase that characterizes the onset of adipocyte differentiation. The image focuses on a single cluster among the wild type cells, and shows a typical field among the BRM-null population. Cell counts from the same populations that showed heightened numbers of alkaline phosphatase positive cells are summarized in the graph below. Wild type BMSC developed an average of 4.25 adipocyte clusters per plate, while the BRM-null BMSC showed none.

Analysis of gene expression (Fig. 5B) in primary non-induced BMSCs shows elevated expression of the alkaline phosphatase gene, *Alpl*, in the BRM-null population consistent with the in situ enzyme activity. A significant increase in *Fgfr2* expression is also apparent. The same RNA was also examined for expression of *Runx2* and osterix, neither of which varied significantly between the wild type and null populations. Of additional note, BRM deficiency in the mice was generated by gene knockout, so the primary cell studies obviate any

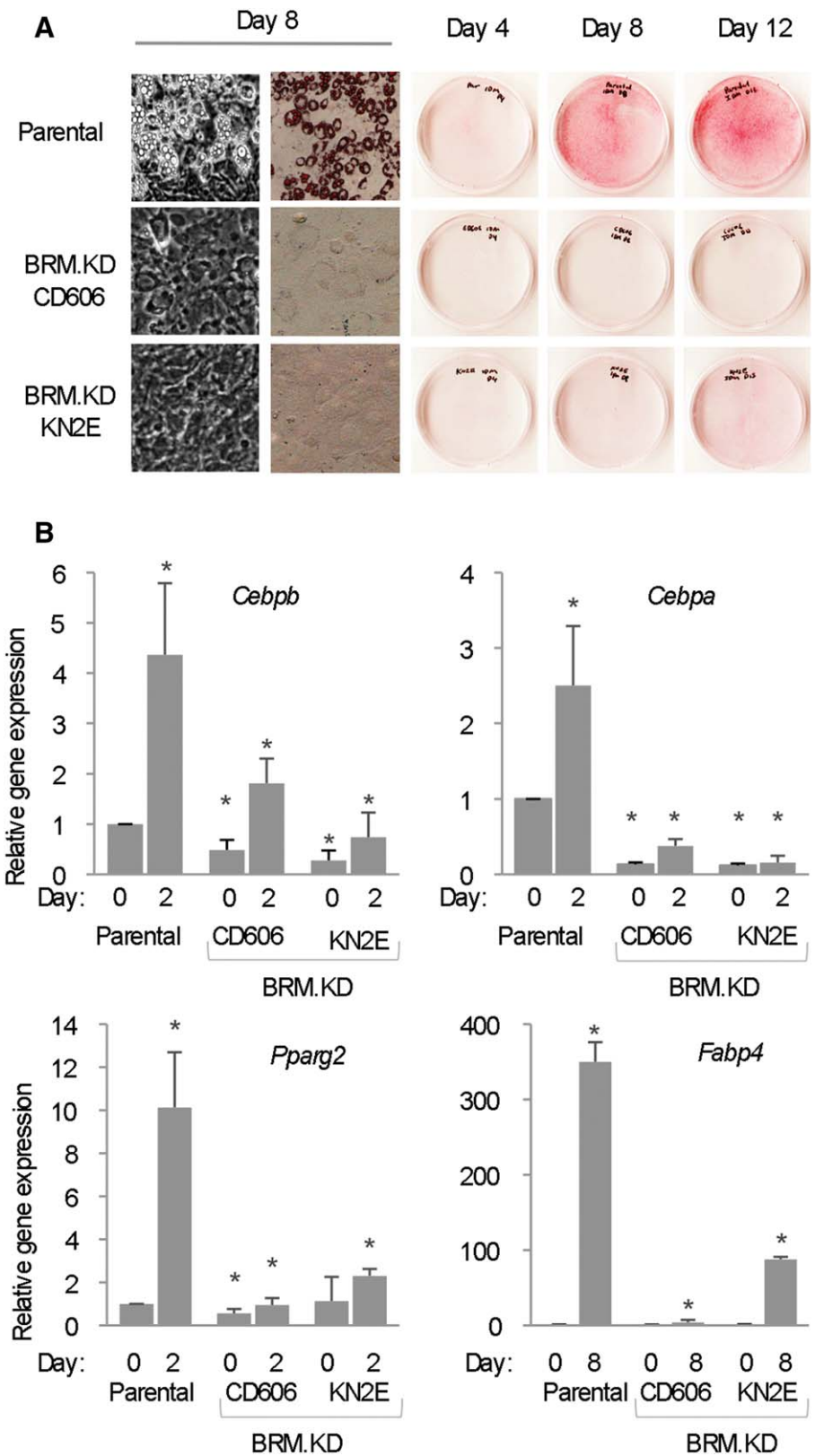

Figure 3. BRM depletion impairs adipogenesis in the C3H10T1/2 mesenchymal stem cell model. **(A):** Induction of the BRM-depleted lines with adipogenic cocktail in parallel with parental C3H10T1/2 cells shows sharply impaired oil red O staining under phase microscopy and on the cell monolayers. Images were captured on an EVOS XL system with a 4× objective. **(B):** BRM-depleted cells show impaired induction of an adipogenic marker panel. Expression was determined by quantitative reverse transcription polymerase chain reaction, normalized to *Gapdh*, and plotted as mean ± SEM. Asterisks indicate a significant difference as described in Figure 1; comparisons are between parental induced and noninduced, and between the knockdown lines and the parental line on the same day.

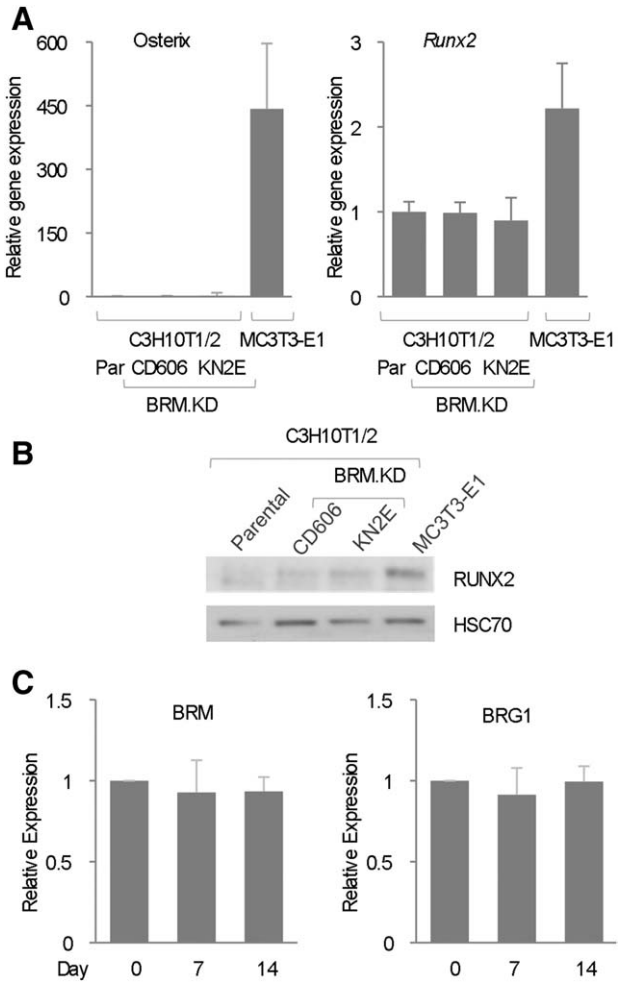

Figure 4. Establishment of commitment in BRM-depleted cells does not lead to further differentiation. **(A):** BRM-depleted cells show no significant induction of osterix or RUNX2 ($p > 0.05$). Expression of osterix and RUNX2 in the pre-osteoblast line, MC3T3-E1 is shown for comparison. Expression was determined by quantitative reverse transcription polymerase chain reaction (qRT-PCR), normalized to *Gapdh*, and plotted as mean ± SEM. **(B):** Visualization of RUNX2 levels by Western blot shows no induction of RUNX2 in BRM-depleted C3H10T1/2 cells; the Runx2 level in MC3T3-E1 pre-osteoblasts is shown for comparison. The constitutively expressed heat shock protein hsc70 was used as a loading control. **(C):** Differentiating MC3T3-E1 cells show no significant change in BRM or BRG1 expression levels ($p > 0.05$) during osteoblast induction. Expression was assessed at time points representative of the pre-osteoblast stage (day 0 of induction), matrix formation (day 7), and late-stage onset of mineralization (day 14). Expression was determined by qRT-PCR, normalized to *Gapdh*, and plotted as mean ± SEM.

concern that off-target effects from RNA interference are driving the cell culture phenotypes.

BRM-Deficient Mice Have Reduced Bone Marrow Adiposity

BRM-null mice must be capable of some degree of adipocyte formation, as their appearance and weight are normal. In vitro approaches are not designed to detect adipocyte formation that might occur slowly, beyond the time-spans typical of cell culture assay parameters, but histological staining can be used to assess actual in situ bone marrow adiposity. The tibias of 12 wild type and 12 BRM-null adult mice, (equal numbers of each sex in each genotype), were harvested for staining with hematoxylin and eosin (H&E), which reveals adipocytes as unstained spheres. The histology shows notably fewer adipocytes in sections from every BRM-null individual than from any wild type individual. Sections of the proximal tibial epiphyses from one individual of each genotype are shown in Figure 6A. Overall cell counts indicate 3.9-fold fewer adipocytes per unit area of bone marrow in the BRM-null mice than detected in the wild type counterparts. Thus, adipocytes do form in the bone marrow of the whole animal in the absence of BRM-SWI/SNF, although in reduced numbers or at a reduced rate. The remaining adipogenic potential in BRM-null mice likely results from sufficient functional overlap with BRG1 to support adipocyte formation at a rate not apparent in time-limited cell culture assays, and helps explain how BRM-null mice are able to maintain normal weight.

BRM-Null Individuals Are Resistant to Age-Related Osteoporosis

An enhanced pool of apparent osteoblast-committed progenitors accompanies the reduced adipocyte potential in BRM-null BMSC. This may be an unused reservoir in healthy individuals, as there is no evidence of ectopic bone formation. While this cell population plays no obvious role in young mice, it might become important when individuals face challenges related to osteoblast deficiency. The most physiological model in which to address this is normal ageing. Loss of cortical bone with advancing age occurs in both mice and humans, in large part due to loss of sufficient osteoblast progenitors over time. Mice reach peak bone mass at about 6 months of age, and by 18 months typically show a dramatic increase in cortical porosity [32].

To compare bone properties with increasing age, micro-computed tomography (micro-CT) analysis was performed on femurs from BRM-null female mice and their wild type counterparts. Images of mid-shaft cross-sections from one individual of each experimental group are shown in Figure 6B, along with group data analysis. Increased cortical porosity with age is readily apparent in the wild type mice (arrow), but is much less evident in BRM-null mice. Quantification shows that cortical porosity in the bones of wild type mice reaches an average of 7.2% by 18 months. BRM-null mice lose far less bone, averaging only 1.8% porosity by the same age. Wild type mice also lost more than 11% mineral density in their cortical tissue by 18 months, while BRM-null mice showed no significant loss. The physiology of mice and humans cannot be compared directly, and measurement parameters are different, but as a point of comparison the loss of mineral density in wild type mice at 18 months is more than 2.5 SDs below the 6-month mean, and the clinical definition of human osteoporosis is a bone mineral density value 2.5 SDs below the young normal [33]. The tissue mineral density of BRM-null mice shows no significant difference from wild type at 6 months, and no significant change by 18 months. This striking protection against age-related bone loss in the BRM-null mice is maintained in the context of overall normal growth. While resistance to osteoporosis relates most directly to available osteoblast progenitors, reduced bone marrow adiposity may make an additional indirect contribution, as bone marrow adipocytes can

secrete cytokines that negatively affect bone formation [34–36].

Discussion

BRM deficiency increases the proportion of committed osteoblast progenitors among BMSCs at the expense of cells with adipogenic potential. BRM-null mice develop normally, but concordant with their increased pool of osteoblast progenitors, these mice show significant resistance to a major consequence of osteoblast insufficiency, that is, age-related osteoporosis. The ability of BRM-null mice to maintain normal bone mineral density argues for the healthy functioning of BRM-null osteoblasts. The influence of BRM on a key lineage decision point in stem cells is a significant new aspect of SWI/SNF function in development. SWI/SNF, in its role as a chromatin-remodeling complex, is a convergent point for signaling from the various hormones, growth factors, and kinase cascades that influence lineage choice in stem cells. BRM acts directly for repression on osteogenic genes [13–15], but contributes primarily to activation of adipogenic factors. Control of osteogenic gene expression appears to be a relatively unusual example of opposing functions between BRM and BRG1. BRG1 is widely required for activation of tissue specific genes [3, 8–12], and is thought to compensate for BRM where their functions overlap [30, 31]. Short-term cell culture systems emphasize functional distinctions, such as the specific role for BRM in adipogenesis, which is not immediately compensated by BRG1 (Figs. 1, 3). However, overlapping gene functions tend to compensate better in long-term animal development, and compensation from BRG1 [6, 30, 31] is the likely reason that BRM-null mice are able to form adipocytes and maintain normal weight. In osteoblastogenesis, BRG1 does not compensate for the repressor role of BRM. However, deficiency of BRM does not lead to uncontrolled differentiation because there are checkpoints independent of SWI/SNF action. Induction of Runx2, is a notable example. BRM and BRG1 have each been recognized in both activation and repression contexts previously, although the alignment with lineage selection seen here is not typical. BRM acts upstream of the major transcription factors associated with the adipocyte/osteoblast decision point (C/EBPα, C/EBPβ, and PPARγ2) and provides a unifying principle in lineage selection without the severe developmental defects that accompany homozygous knockout of these factors.

The intrinsic effect of signaling from FGFR2 was recognized from human mutations that cause constitutive activation of the tyrosine kinase activity. These activating mutations signal precocious differentiation of osteoblasts, overtly evident in mice and humans as distinctive changes in skull shape due to early closure at the pre-osteoblast-rich borders of the cranial sutures [26, 27, 37]. FGFR2 signaling is now understood to

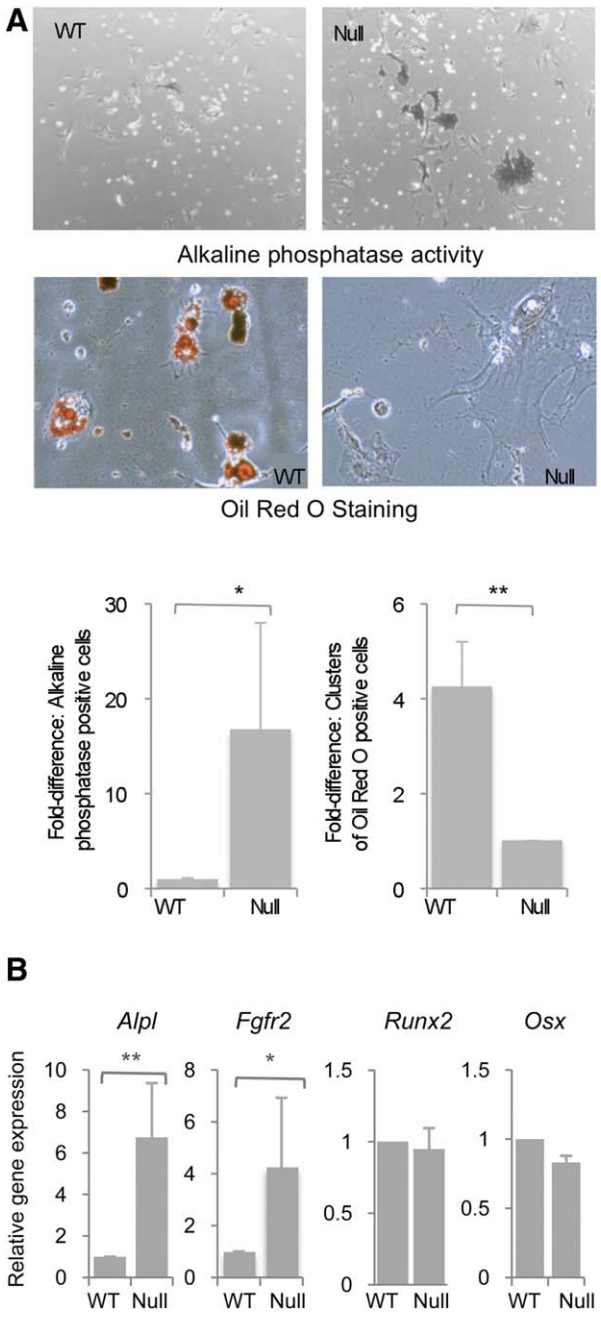

Figure 5. Enhanced osteoblast markers and impaired adipogenesis in primary BMSC from BRM-null mice. The primary BMSC pool from BRM-null mice shows increased expression of markers of osteoblast progenitor status and reduced adipogenic potential. **(A):** Primary BMSC from BRM-null mice, without induction, contain more alkaline phosphatase-positive cell clusters than BMSC from their wild type counterparts (upper panels). Aliquots of the same cell population show reduced adipogenic potential (lower panels). Images were captured on an EVOS XL system with a 10× objective. The figure focuses on a single cluster of adipocytes among the wild type cells, and a typical field among the BRM-null population. The images are representative of four independent experiments with four different cell preparations. Cell counts across the four experiments showed on average 16.8-fold more alkaline phosphatase positive cells among BRM-null BMSCs compared with wild type. When induced for adipogenesis, the wild type cell population showed on average 4.25 clusters of oil red O positive cells per plate, while BRM-null cells showed no clear positives; to express this as a ratio would require division by zero, but it indicates a 4.25-fold minimal difference. *, $p < 0.05$; **, $p < 0.01$. **(B):** Expression of *Alpl* and *Fgfr2* is elevated in BMSC from BRM-null mice relative to their wild type counterparts, while expression of *Runx2* and osterix (*Sp7*) does not change significantly with BRM knockdown. Expression was measured by quantitative reverse transcription polymerase chain reaction, normalized to *Gapdh* expression, and plotted as mean ± SEM. *, $p < 0.05$; **, $p < 0.01$. Abbreviation: WT, wild type.

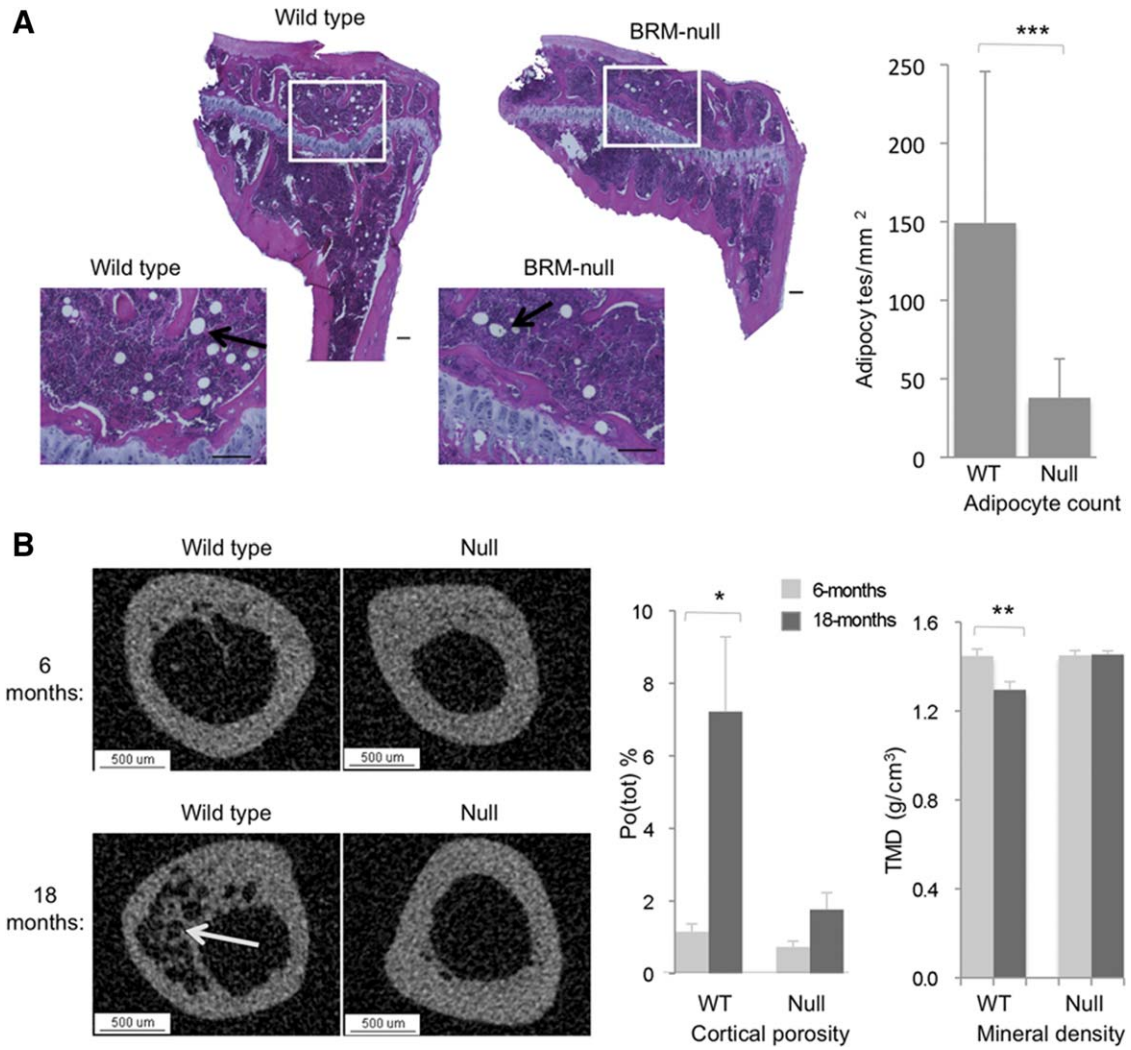

Figure 6. Reduced bone marrow adiposity and resistance to age-related osteoporosis in BRM-null mice. **(A):** H&E staining of decalcified tibias reveals adipocytes as unstained spheres in the proximal tibial condyle. Scale bars = 100 μm. The boxed region is enlarged to show the adipocytes (arrows) more clearly. Twelve individuals of each genotype (equal numbers of males and females) aged 4 months were analyzed. Representative condyle sections and enlarged insets from the growth-plate region are shown for one male of each genotype. Quantification across all samples shows on average 3.9-fold fewer adipocytes per unit area of bone marrow in the BRM-null mice compared with wild type. Data are plotted as mean ± SEM ($n = 12$). ***, $p < 0.001$. **(B):** Cross-sectional micro-CT imaging of female right femurs reveals increasing cortical porosity (arrow) in wild type mice at 18 months compared with 6 months; the BRM-null mice develop markedly less cortical porosity over a similar time span. Scale bars = 500 μm. Quantification across all samples shows an increase in porosity to 7.2% in the wild-type (wt) mice with 11.1% loss of tissue mineral density (TMD). *, $p < 0.05$; **, $p < 0.01$. BRM-null mice lose far less bone, averaging only 1.8% porosity at 18 months, a difference from the 6-month value with borderline statistical significance ($p = 0.050$). There was no detectable loss of TMD with age in the BRM-null mice. Data are plotted as mean ± SEM (6 month $n = 4$; 18 month $n = 5$). The mean mineral density of wild type mice at 6 months is 1.46 g/cm^3 (SD = 0.06). The drop to 1.3 g/cm^3 at 18 months represents a loss of more than 2.5 SDs.

play an important role in osteogenesis from lineage selection to osteoblast maturation [28, 38, 39]. Vertebrates express at least 22 different FGF ligands, and at least half of these can signal through FGFR2. Ligand-mediated activation of the receptor in vivo depends on the balance of FGFs, and on the distinct timing and location of their expression patterns [38, 39]. Increased expression of FGFR2 with BRM deficiency is consistent across the two independently generated knockdown lines and the primary cell model. Elevated expression of *Fgfr2* is not equivalent to constitutive activation, and the increased osteoblast progenitor pool in BRM-null mice does not result in craniofacial malformations. The resistance to age-related osteoporosis in BRM-null mice implies that their increased osteoblast progenitor pool is able to persist as a stable reservoir that differentiates only according to normal physiological signals, and thus becomes significant only upon challenges related to osteoblast deficiency. The lack of induction of RUNX2 and osterix in BRM-depleted stem cells supports the interpretation that the BRM-deficient stem cell pool contains an increased proportion of osteoblast progenitors maintained at the commitment stage. A controlled shift to commitment without undergoing further differentiation may be a particular advantage of influencing lineage selection through SWI/SNF. As a normal focal point for the complex array of signals influencing gene expression during differentiation, SWI/SNF may provide a more physiological level of programmatic control. Control of osteogenic genes by BRM-SWI/SNF also acts at

points downstream of induction of RUNX2 and osterix. In the MC3T3-E1 pre-osteoblast model, where RUNX2 and osterix are already actively expressed, BRM depletion permits early induction of mid-late stage osteoblast markers including osteocalcin and MSX1. This still does not cause differentiation to the mature osteoblast phenotype, although it does enhance the rate of progression to mineralization [13].

During osteoblast development, BRM repression of osteogenic genes is relieved by dissociation of the BRM complex from promoters such as *Alpl* [13–16]. BRM is not downregulated in normal osteogenesis, but targeting BRM could be a novel therapeutic strategy for promoting bone formation, with the advantage of the remarkable lack of overt pathology in BRM-null mice.

The major phenotypic variation reported in the mice before this study is prostate hyperplasia, associated with a specific role of BRM as a coregulator of the androgen receptor [40]. BRM is epigenetically silenced in a wide range of tumors [30, 31], and BRM-null mice are sensitive to carcinogen-induced tumors [41, 42], but the mice do not show increased spontaneous susceptibility to cancer [6, 30, 31], and BRM has actually been identified as a target for cancer treatment, discussed further below. Developmental changes linked with BRM insufficiency are surprisingly few. Polymorphisms in the human BRM-encoding gene (*Smarca2)* that impair expression or nuclear localization of BRM are suggested risk factors for schizophrenia [43, 44], and BRM-null mice show mild neurological changes [44]. Nicolaides-Baraitser syndrome, which is characterized by sparse hair and distinctive facial and musculoskeletal features, was recently linked with heterozygous missense mutations in *Smarca2* [45, 46]. However, the mutations, which cause small amino acid changes in the ATPase domain, appear to have gain-of-function effects rather than loss of function. No comparable developmental effects are evident in BRM knockout mice. Smooth muscle development has also been examined in BRM-null mice; the effects of conditional BRG1 knockout were exacerbated in a BRM-null background, but morphology was normal in BRM-null mice when BRG1 was not targeted [11]. The conservation of BRM in higher eukaryotes argues that BRM is specifically advantageous along with BRG1 in mammalian development, but lack of BRM seems relatively benign overall, and there would likely be few deleterious side effects from targeting BRM for bone regeneration.

Certain orthopedic applications are potential front-line choices for gene targeting by RNA silencing or gene editing because they use autologous bone marrow grafts, which can be treated directly ex vivo, and require only short-term efficacy. These features obviate the two biggest obstacles to therapeutic gene silencing applications, that is, inability to target the desired tissues/cells directly, and inability to sustain the silencing effects for the long-term.

Systemic targeting of BRM for applications such as osteoporosis would likely require small molecule inhibitors that would need to be specific with respect to the closely related protein BRG1. Incentive to develop BRM inhibitors is increased by recent evidence that BRM can be targeted as a synthetic-lethal strategy against BRG1-negative cancers [47–49]. Potential target sites in BRM include the relatively nonconserved N-terminal region and C-terminal acetylation sites, both of which are structure/function sites distinct to BRM versus BRG1 [50, 51].

Conclusion

Controlled lineage selection in bone marrow stroma-derived mesenchymal stem cells is an attractive approach for cell engineering and tissue regeneration. The finding that the balance of the osteoblast/adipocyte progenitor selection point in these cells is strongly influenced by BRM levels has broad translational potential and may open other doors to precision control of stem cell fate by SWI/SNF.

Acknowledgments

We thank the support of Dr. Fred F. Buechel, and also Dr. Karen Knudsen for the generous gift of breeding pairs of the BRM knockout mice, and the Institut Pasteur for permission to use them. This work was supported by the National Institute of General Medical Sciences, the National Institute of Arthritis and Musculoskeletal and Skin Diseases, and the National Cancer Institute of the National Institutes of Health under Grants R01GM073257 (to E.M.), R21-AR063351 (to J.C.F.), and T32-CA134268 (to S.F.); and a Translational Research Award from the Foundation of UMDNJ (now NJ Health Foundation).

Author Contributions

K.H.N. and S.F.: collection and assembly of data, experimental design, data analysis and interpretation; F.X.: collection and assembly of data, experimental design, data analysis and interpretation, manuscript writing; E.A.J.W.: collection of data; J.C.F.: data analysis and interpretation; E.M.: experimental conception and design; data analysis and interpretation, manuscript writing. K.H.N., F.X., and S.F. contributed equally to this article.

Disclosure of Potential Conflicts of Interest

S.F. and E.M. are authors on US Patent 8415316, whose value could be affected by publication. All other authors indicate no potential conflicts of interest.

References

1 Verma S, Rajaratnam JH, Denton J et al. Adipocytic proportion of bone marrow is inversely related to bone formation in osteoporosis. J Clin Pathol 2002;55:693–698.

2 Nuttall ME, Gimble JM. Controlling the balance between osteoblastogenesis and adipogenesis and the consequent therapeutic implications. Curr Opin Pharmacol 2004;4: 290–294.

3 Wu JI. Diverse functions of ATP-dependent chromatin remodeling complexes in development and cancer. Acta Biochim Biophys Sin (Shanghai). 2012 44: 54–69.

4 Mehrotra A, Mehta G, Aras S et al. SWI/SNF Chromatin Remodeling Enzymes in Melanocyte Differentiation and Melanoma. Crit Rev Eukaryot Gene Expr 2014;24: 151–161.

5 Narayanan R, Tuoc TC. Roles of chromatin remodeling BAF complex in neural differentiation and reprogramming. Cell Tissue Res 2014;356:575–584.

6 Reyes JC, Barra J, Muchardt C et al. Altered control of cellular proliferation in the

absence of mammalian brahma (SNF2alpha). EMBO J 1998;17:6979–6991.
7 Bultman SJ, Gebuhr T, Yee D et al. A Brg1 null mutation in the mouse reveals functional differences among mammalian SWI/SNF complexes. Mol Cell 2000;6:1287–1295.
8 Young DW et al. SWI/SNF chromatin remodeling complex is obligatory for BMP2-induced, Runx2-dependent skeletal gene expression that controls osteoblast differentiation. J Cell Biochem 2005;94:720–730.
9 de la Serna IL, Ohkawa Y, Imbalzano AN. Chromatin remodelling in mammalian differentiation: Lessons from ATP-dependent remodellers. Nat Rev Genet 2006;7:461–473.
10 Griffin CT, Brennan J, Magnuson T. The chromatin-remodeling enzyme BRG1 plays an essential role in primitive erythropoiesis and vascular development. Development 2008;135:493–500.
11 Zhang M, Chen M, Kim JR et al. SWI/SNF complexes containing Brahma or Brahma-related gene 1 play distinct roles in smooth muscle development. Mol Cell Biol 2011;31:2618–2631.
12 Narayanan R, Tuoc TC. Roles of chromatin remodeling BAF complex in neural differentiation and reprogramming. Cell Tissue Res 2014;356:575–584.
13 Flowers S, Nagl NG Jr, Beck GR Jr et al. Antagonistic roles for BRM and BRG1 SWI/SNF complexes in differentiation. J Biol Chem 2009;284:10067–10075.
14 Flowers S, Beck GR Jr, Moran E. Tissue-specific gene targeting by the multiprotein mammalian DREAM complex. J Biol Chem 2011;286:27867–27871.
15 Xu F, Flowers S, Moran E. Essential role of ARID2 protein-containing SWI/SNF complex in tissue-specific gene expression. J Biol Chem 2012; 287:5033–5041.
16 Flowers S, Xu F, Moran E. Cooperative activation of tissue specific genes by pRB and E2F1. Cancer Res 2013;73:2150–2158.
17 Pedersen TA, Kowenz-Leutz E, Leutz A et al. Cooperation between C/EBPalpha TBP/TFIIB and SWI/SNF recruiting domains is required for adipocyte differentiation. Genes Dev 2001;15:3208–3216.
18 Salma N, Xiao H, Mueller E et al. Temporal recruitment of transcription factors and SWI/SNF chromatin-remodeling enzymes during adipogenic induction of the peroxisome proliferator-activated receptor gamma nuclear hormone receptor. Mol Cell Biol 2004;24:4651–4663.
19 Caramel J, Medjkane S, Quignon F et al. The requirement for SNF5/INI1 in adipocyte differentiation highlights new features of malignant rhabdoid tumors. Oncogene 2008;27:2035–2044.
20 Rosen ED, MacDougald OA. Adipocyte differentiation from the inside out. Nat Rev Mol Cell Biol 2006;7:885–896.
21 Tang, QQ, Lane, MD. Adipogenesis: From stem cell to adipocyte. Annu Rev Biochem 2012;81:715–736.
22 Akune T, Ohba S, Kamekura S et al. PPARgamma insufficiency enhances osteogenesis through osteoblast formation from bone marrow progenitors. J Clin Invest 2004;113:846–855.
23 Takada I, Suzawa M, Matsumoto K et al. Suppression of PPAR transactivation switches cell fate of bone marrow stem cells from adipocytes into osteoblasts. Ann N Y Acad Sci 2007;1116:182–195.
24 Kawai M, Sousa KM, MacDougald OA et al. The many facets of PPARgamma: Novel insights for the skeleton. Am J Physiol Endocrinol Metab 2010;299: E3–E9.
25 Katagiri T, Yamaguchi A, Ikeda T et al. The non-osteogenic mouse pluripotent cell line, C3H10T1/2, is induced to differentiate into osteoblastic cells by recombinant human bone morphogenetic protein-2. Biochem Biophys Res Commun 1990;172:295–299.
26 Du X, Xie Y, Xian CJ et al. Role of FGFs/FGFRs in skeletal development and bone regeneration. J Cell Physiol 2012;227: 3731–3743.
27 Marie PJ, Miraoui H, Sévère N. FGF/FGFR signaling in bone formation: Progress and perspectives. Growth Fact 2012;30:117–123.
28 Miraoui H, Oudina K, Petite H et al. Fibroblast growth factor receptor 2 promotes osteogenic differentiation in mesenchymal cells via ERK1/2 and protein kinase C signaling. J Biol Chem 2009;284:4897–4904.
29 Long F. Building strong bones: Molecular regulation of the osteoblast lineage. Nat Rev 2012;13:27–38.
30 Reisman D, Glaros S, Thompson EA. The SWI/SNF complex and cancer . Oncogene 2009; 28: 1653–1668.
31 Wilson BG, Roberts CW. SWI/SNF nucleosome remodellers and cancer. Nat Rev Cancer. 2011;11:481–492.
32 Jilka RL. The relevance of mouse models for investigating age-related bone loss in humans. J Gerontol A Biol Sci Med Sci 2013;68:1209–1217.
33 Kanis JA, McCloskey EV, Johansson H et al. A reference standard for the description of osteoporosis. Bone 2008;42:467–475.
34 Kawai M, de Paula FJ, Rosen CJ. New insights into osteoporosis: The bone-fat connection. J Intern Med 2012;272:317–329.
35 Liu Y, Song CY, Wu SS et al. Novel adipokines and bone metabolism. Int J Endocrinol 2013;2013:895045.
36 Sadie-Van Gijsen H, Crowther NJ, Hough FS et al. The interrelationship between bone and fat: From cellular see-saw to endocrine reciprocity. Cell Mol Life Sci 2013;70:2331–2349.
37 Perlyn CA, DeLeon VB, Babbs C et al. The craniofacial phenotype of the Crouzon mouse: Analysis of a model for syndromic craniosynostosis using three-dimensional MicroCT. Cleft Palate Craniofac J 2006;43:740–748.
38 Katoh M. FGFR2 abnormalities underlie a spectrum of bone, skin, and cancer pathologies. J Invest Dermatol 2009;129:1861–1867.
39 Xie Y, Zhou S, Chen H et al. Recent research on the growth plate: Advances in fibroblast growth factor signaling in growth plate development and disorders. J Mol Endocrinol 2014;53:T11–T34.
40 Shen H, Powers N, Saini N et al. The SWI/SNF ATPase Brm is a gatekeeper of proliferative control in prostate cancer. Cancer Res 2008;68:10154–10162.
41 Halliday GM, Zhou Y, Sou PW et al. The absence of Brm exacerbates photocarcinogenesis. Exp Dermatol 2012;21:599–604.
42 Glaros S, Cirrincione GM, Muchardt C et al. The reversible epigenetic silencing of BRM: Implications for clinical targeted therapy. Oncogene 2007;26:7058–7066.
43 Walsh T, McClellan JM, McCarthy SE et al. Rare structural variants disrupt multiple genes in neurodevelopment pathways in schizophrenia. Science 2008;320:539–543.
44 Koga M, Ishiguro H, Yazaki S et al. Involvement of SMARCA2/BRM in the SWI/SNF chromatin-remodeling complex in schizophrenia. Hum Mol Genet 2009;18:2483–2494.
45 Van Houdt JK, Nowakowska BA, Sousa SB et al. Heterozygous missense mutations in SMARCA2 cause Nicolaides-Baraitser syndrome. Nat Genet 2012;44:445–449.
46 Wolff D, Endele S, Azzarello-Burri S et al. In-Frame Deletion and Missense Mutations of the C-Terminal Helicase Domain of SMARCA2 in Three Patients with Nicolaides-Baraitser Syndrome. Mol Syndromol 2012;2:237–244.
47 Oike T, Ogiwara H, Tominaga Y et al. A synthetic lethality-based strategy to treat cancers harboring a genetic deficiency in the chromatin remodeling factor BRG1. Cancer Res 2013;73:5508–5518.
48 Hoffman GR, Rahal R, Buxton F et al. Functional epigenetics approach identifies BRM/SMARCA2 as a critical synthetic lethal target in BRG1-deficient cancers. Proc Natl Acad Sci USA 2014;111:3128–3133.
49 Wilson BG, Helming KC, Wang X et al. Residual complexes containing SMARCA2 (BRM) underlie the oncogenic drive of SMARCA4 (BRG1) mutation. Mol Cell Biol 2014;34:1136–1144.
50 Kadam S, Emerson BM. Transcriptional specificity of human SWI/SNF BRG1 and BRM chromatin remodeling complexes. Mol Cell 2003;11:377–389.
51 Bourachot B, Yaniv M, Muchardt C. Growth inhibition by the mammalian SWI-SNF subunit Brm is regulated by acetylation. EMBO J 2003;22: 6505–6515.